Nanoscale

ROYAL SOCIETY OF CHEMISTRY

PAPER

View Article Online
View Journal | View Issue

Cite this: *Nanoscale*, 2023, **15**, 10677

Defect passivation and electron band energy regulation of a ZnO electron transport layer through synergetic bifunctional surface engineering for efficient quantum dot light-emitting diodes†

Fensha Cai, [a] Yufei Tu,[b] Dadi Tian,[a] Yan Fang,[a] Bo Hou, [c] Muhammad Ishaq,[d] Xiaohong Jiang,[a] Meng Li, [a] Shujie Wang*[a] and Zuliang Du *[a]

Zinc oxide nanoparticles (ZnO NPs) have been actively pursued as the most effective electron transport layer for quantum-dot light-emitting diodes (QLEDs) in light of their unique optical and electronic properties and low-temperature processing. However, the high electron mobility and smooth energy level alignment at QDs/ZnO/cathode interfaces cause electron over-injection, which aggravates non-radiative Auger recombination. Meanwhile, the abundant defects hydroxyl group (–OH) and oxygen vacancies (O_V) in ZnO NPs act as trap states inducing exciton quenching, which synergistically reduces the effective radiation recombination for degrading the device performance. Here, we develop a bifunctional surface engineering strategy to synthesize ZnO NPs with low defect density and high environmental stability by using ethylenediaminetetraacetic acid dipotassium salt (EDTAK) as an additive. The additive effectively passivates surface defects in ZnO NPs and induces chemical doping simultaneously. Bifunctional engineering alleviates electron excess injection by elevating the conduction band level of ZnO to promote charge balance. As a result, state-of-the-art blue QLEDs with an EQE of 16.31% and a T_{50}@100 cd m^{-2} of 1685 h are achieved, providing a novel and effective strategy to fabricate blue QLEDs with high efficiency and a long operating lifetime.

Received 15th March 2023,
Accepted 21st May 2023

DOI: 10.1039/d3nr01194a

rsc.li/nanoscale

1. Introduction

Quantum dot light-emitting diodes (QLEDs) featuring cost-effective electroluminescence, wide-color gamut, and high color purity are high-potential candidates for next-generation displays.[1–5] Indeed, progress in this area has been dramatic; the external quantum efficiency (EQE) of red, green, and blue QLEDs has reached 30.9%, 28.7%, and 21.9%, respectively.[6,7] In addition, the T_{95} operating lifetimes (the time for the brightness to decrease to 95% of the initial brightness) of the three primary colors reached 7668, 7500, and 57 h at an initial brightness of 1000 cd m^{-2}, respectively.[7,8] Obviously, the performance of blue QLEDs is lower than that of their green and red counterparts. The main reason is that the deep valence band levels of the blue QD emitting layer (EML) increase the hole injection barrier, thus leading to an imbalance of holes and electrons. Unbalanced carrier injection induces Auger recombination, thus affecting the device efficiency and lifetime. Therefore, it is indispensable to achieve both high-efficiency and long-lifetime blue QLEDs.

For the state-of-the-art QLED device, ZnO NPs are the most commonly employed as the electron transport layer (ETL) because of their high electron mobility and optimal energy band alignment.[9–11] However, QLEDs with the ZnO ETL generally lead to charge imbalance in the QDs due to a non-negligible energetic barrier for hole injection. Consequently, the over-accumulation of electrons at the hole transport layer (HTL) and QD interface leads to increasing non-radiative Auger recombination.[12] Additionally, low-temperature processed ZnO NPs exhibit a relatively open hexagonal close-packed lattice structure with the Zn atoms occupying only half of the tetrahedral sites, which therefore lead to trap states of Zn interstitials (Zn_i) and O_V.[13,14]

[a]*Key Lab for Special Functional Materials of Ministry of Education, National & Local Joint Engineering Research Center for High-efficiency Display and Lighting Technology, School of Materials Science and Engineering, and Collaborative Innovation Center of Nano Functional Materials and Applications, Henan University, Kaifeng 475004, China. E-mail: wsj@henu.edu.cn, zld@henu.edu.cn*
[b]*School of Electronics Information and Intelligent Manufacturing, Sias University, Xinzheng, China*
[c]*School of Physics and Astronomy, Cardiff University, Cardiff, Wales, CF24 3AA, UK*
[d]*Institute of Fundamental and Frontier Sciences, University of Electronic Science and Technology of China, Chengdu 610054, China*

† Electronic supplementary information (ESI) available. See DOI: https://doi.org/10.1039/d3nr01194a

Previous reports revealed that –OH defects exist on the surface of ZnO NPs during the solution process.[15] All these defects could act as charge-trapping centers, resulting in exciton quenching at the QD/ETL interface.[16,17]

In view of the aforementioned issues, various strategies have been proposed to balance charge injection and suppress interfacial exciton quenching. For instance: inserting insulating layers such as poly(methyl methacrylate) (PMMA),[18] poly-[(9,9-bis(30-(*N*,*N*-dimethylamino) propyl)-2,7-fluorene)-*alt*-2,7-(9,9-dioctylfluorene)] (PFN),[19] Al_2O_3 [20] and polyethylenimine (PEI)[21] between QDs and the ETL; doping ZnO NPs with metal elements including Mg,[22] Li,[23] Al,[24] Sn,[25] Be,[26] and Ga;[27] altering the surface of ZnO NPs with organic materials.[28–31] Although these strategies can improve the device performance, it is challenging to precisely adjust the thickness of the ultrathin interlayer. A thin interlayer is ineffective in blocking electrons and can even have tunneling effects that promote electron injection. A thick interlayer increases resistance and isolates charge transport. In addition, doped ZnO NP solutions appear to be particularly chemically reactive and have a propensity to agglomerate in the environment.[32] Therefore, in order to reduce electron over-injection and improve stability, techniques that can simultaneously control energy levels and passivate defects in ZnO NPs must be developed.

Here, we present a bifunctional strategy that uses EDTAK to tailor ZnO (EK-ZnO) as the ETL in blue QLEDs with improved efficiency and operational stability. The detailed analysis indicates that EDTAK can significantly passivate –OH and O_V defects to relieve exciton quenching. The chemical interaction contributes to upshifting the conduction band minimum (CBM) of ZnO to impede the injection of excess electrons. Meanwhile, the stability of ZnO NPs is increased due to the chelation function of EDTAK. Utilizing such bifunctional EK-ZnO as the ETL, the fabricated QLED displays the peak luminance value of 20060 cd m^{-2} and the EQE value of 16.31%. Peak values and EQE both improved by 42% and 53% over the control device, respectively. The device operating stability (T_{50}@100 cd m^{-2}) is enhanced by 10-fold from 170 h to 1685 h. The proposed strategy in this manuscript highlights enormous potential for developing highly reliable and efficient QLEDs and other optoelectronic devices.

2. Results and discussion

ZnO NPs were synthesized by the sol–gel method according to our previous work.[22] Typically, zinc acetate dihydrate ($Zn(OAc)_2{\cdot}2H_2O$) in dimethyl sulfoxide (DMSO) solution was mixed with tetramethylammonium hydroxide (TMAH) in ethanol solution. The mixture was stirred for 1 hour to generate ZnO nanocrystals, followed by precipitation with a mixed solution of ethanol and *n*-hexane and then re-dispersion in ethanol. Regarding EK-ZnO NPs, EDTAK in methyl alcohol solution was added (Fig. S1†) in the mixed solution of $Zn(OAc)_2{\cdot}2H_2O$ and TMAH. The solution was stirred for 1 hour and re-dispersed in ethanol (details are discussed in the Experimental section). The presence of N 1s and K 2p peaks for the EK-ZnO sample from X-ray photoelectron spectroscopy (XPS) measurements (Fig. 1a and S2†) confirmed the incorporation of additives on the surface of the functionalized ZnO films.[33] An obvious red-shift absorption spectrum of EK-ZnO NPs shown in Fig. 1b authenticates the doping of K^+ in ZnO NPs. The acquired K^+ doping also caused a little increase in the grain size of ZnO NPs (from 4.23 nm to 4.37 nm), which might be assigned to the occupation of O_V in ZnO NPs by K^+,[34] as seen in the TEM measurements (Fig. S3†). Fourier transform infrared (FTIR) spectroscopy was performed to further investigate the chemical interaction between ZnO and EDTAK. The peak around 2960 cm^{-1} corresponding to the C–H stretching vibration in EDTAK molecules was observed in EK-ZnO, indicating successful introduction of additives in the ZnO film (Fig. S4†).[34] The peak around 1641.3 cm^{-1} in EDTAK corresponded to the C=O stretching vibration, while it disappeared in EK-ZnO. The stretching vibration of the O–C–O bond also manifested as an additional peak at 1590.4 cm^{-1} (Fig. 1c).[31,35] The conversion from C=O to O–C–O stretching vibration demonstrated a significant reduction of oxygen-bearing groups such as the –OH group.[31] As a previous literature report, the –OH group binding to one metal site showed a basic characteristic, and the –COOH group from EDTAK showed an acidic characteristic.[15,33] Therefore, an acid–base neutralization reaction occurred, reducing oxygen-containing groups such as –OH on the surface of ZnO NPs. A typical wurtzite-type ZnO structure could be seen in the XRD patterns of ZnO and EK-ZnO NPs (Fig. 1d). The absence of any peak shifts and additive peaks in EK-ZnO films demonstrated a small amount of additive accumulation in EK-ZnO films.[34]

Furthermore, atomic force microscopy (AFM) was carried out to study the surface topography of ZnO and EK-ZnO film surfaces deposited on bare glass. As shown in Fig. S5,† the root-mean-square (RMS) values of both samples showed negligible changes, suggesting a uniform coverage of the surface of ZnO films with no agglomeration and it was pinhole-free.

To investigate the passivation effect of additive molecules on typical defects such as –OH and O_V of ZnO NPs, we characterized the steady state PL of ZnO and EK-ZnO solutions. The PL emission peaks around 375 nm were ascribed to near-band-edge emission, which originated from intrinsic luminescence of ZnO exciton recombination.[22,29] The peaks around 524 nm were ascribed to defect state emission such as O_V, –OH and interstitial oxygen generated during the synthesis.[36] The defect state emission might have originated from the photo-excited electrons in the CBM of ZnO relaxing to the mid-gap defect states and recombining radiatively to the holes in the valence band.[37] The defect state emission intensity could reflect the density of defect states to a certain degree.[38] According to Fig. 2a, the additive molecules could successfully passivate the defects and lower the defect density in ZnO NPs by reducing the PL intensity of defect state emission and increasing near-band-edge emission (375 nm).

To further elucidate the defect's passivation effect, we performed X-ray photoemission spectroscopy (XPS) to analyze the

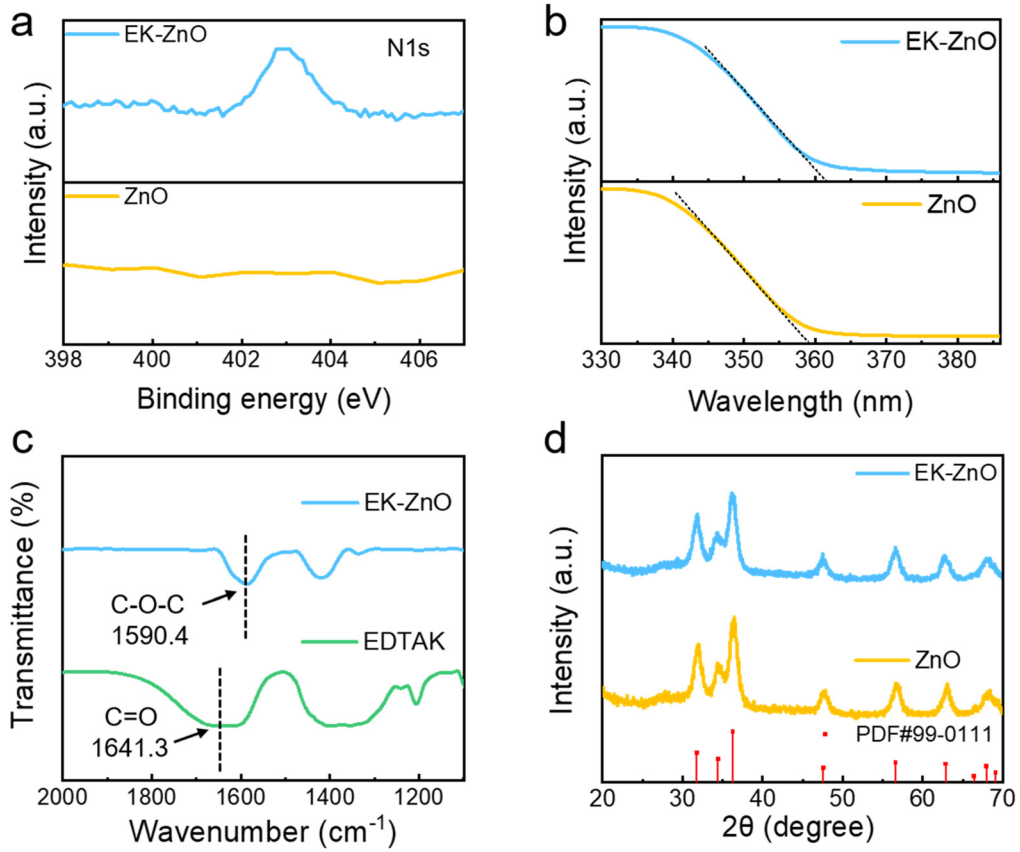

Fig. 1 (a) XPS spectra of N 1s, (b) UV-vis absorption spectra, (c) FTIR spectra and (d) XRD patterns of ZnO and EK-ZnO films.

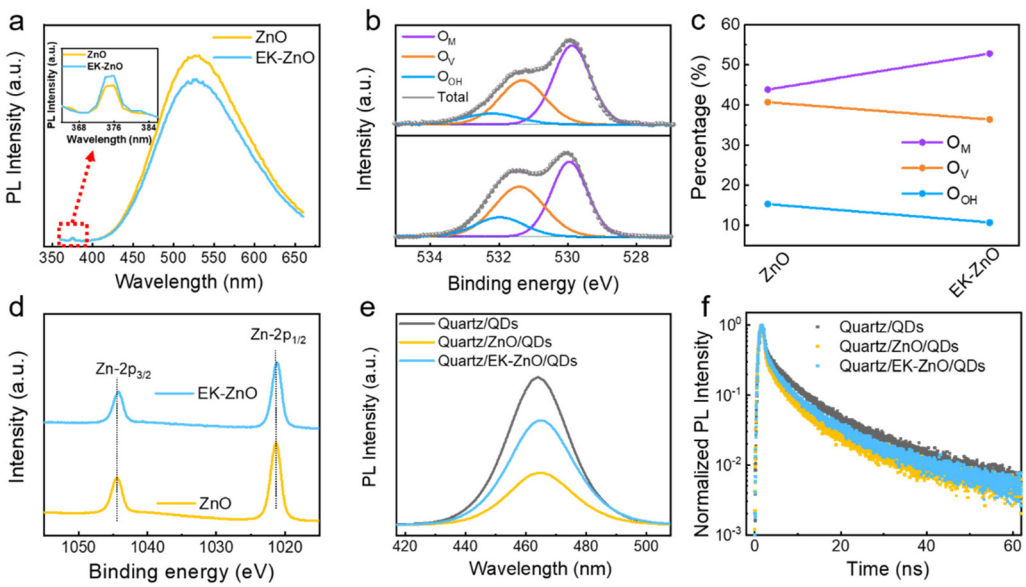

Fig. 2 (a) Steady-state PL spectra of ZnO and EK-ZnO solution, inset: the locally amplified PL spectrum in the ultraviolet region. XPS spectra of (b) O 1s, (d) Zn 2p ZnO and EK-ZnO films. (c) The percentages of O_{OH}, O_V, and O_M extracted from the results of the XPS spectra of O 1s. (e) Steady-state PL spectrum and (f) time-resolved PL decay curves of QD films on quartz, ZnO and EK-ZnO substrates.

binding energy of Zn 2p and O 1s core levels before and after EDTAK modification. As shown in Fig. 2b, the O ls core level spectra were deconvoluted with Gaussian peaks for identifying the change after modification with EDTAK. Both pristine ZnO and EK-ZnO surfaces exhibited a peak at ~530.0 eV corresponding to the metal oxide (O_M). The shoulders at ~531.4 and ~532.0 eV were assigned to O_V and O_{OH}, respectively.[30,34,39] The percentages for these species are summarized in Fig. 2c, which clearly shows that both O_V and O_{OH} attenuate distinctly, accompanied by an increase in O_M. The XPS results and FTIR analyses demonstrated the deprotonation of carboxyl in EDTAK reacted with the surface-OH defects and K-doped passivation of the O_V defects. Notably, the Zn 2p peaks of EK-ZnO presented a slight shift to a lower binding energy compared with the unmodified samples, further suggesting a chemical interaction between the ZnO NPs and additive molecules.[31]

To confirm the passivation effects of EDTAK, we performed steady-state PL and time-resolved PL decay (TRPL) measurements for QD films on quartz, ZnO and EK-ZnO substrates, respectively. QD films on ZnO and EK-ZnO exhibited weaker PL emission compared with that on quartz, consistent with the exciton quenching at the QD/ZnO interface by defect capturing. The quartz/QDs/EK-ZnO sample showed stronger PL emission than the quartz/QDs/ZnO sample. This implies reduced quenching of QDs at the interface resulting increased radiative recombination. The average exciton lifetime (τ_{avg}) was extracted by a bi-exponential fitting function.[40] τ_{avg} was rapidly reduced to 4.35 ns for quartz/QDs/ZnO relative to 5.88 ns for quartz/QDs, and then was gradually increased to 5.13 ns in the EK-ZnO sample (Table S1†), indicating that the present additives were effective in suppressing the interfacial non-radiative recombination at the QDs/ZnO interface.

Based on these observations, the passivation effect was attributed to the chemical interaction between the ZnO NPs and additive molecules. Reduction of surface –OH defects *via* an acid–base neutralization reaction and O_V defects was induced by K^+ doping into ZnO simultaneously, which will tune the energy-level alignment at this interface.[33,34] These changes were revealed by the UV-vis absorption spectra and ultraviolet photoemission spectroscopy (UPS) analysis.

The UV-vis absorption spectra demonstrated an optical band gap (E_g) of 3.52 eV for ZnO and 3.49 eV for EK-ZnO, consistent with previous reports (Fig. 3a).[41,42] Fig. 3b shows the secondary photoelectron cutoff ($E_{cut\text{-}off}$) and valence band region (E_{onset}) for ZnO and EK-ZnO. The work functions (WF) of pristine ZnO and EK-ZnO were determined to be 3.80 and 3.53 eV, respectively, using the equation: $W_F = 21.22 - E_{cutoff}$.[43] Combined with band gap, the CBM of pristine ZnO and EK-ZnO were found to be −3.97 and −3.69 eV, respectively, which is demonstrated in the corresponding energy level diagram (Fig. 3c). An increased energy barrier for electron transport at the EK-ZnO/Al interface impedes injection of excess electrons and facilitates charge balance in the device. Meanwhile, the CBM of EK-ZnO was slightly higher than that

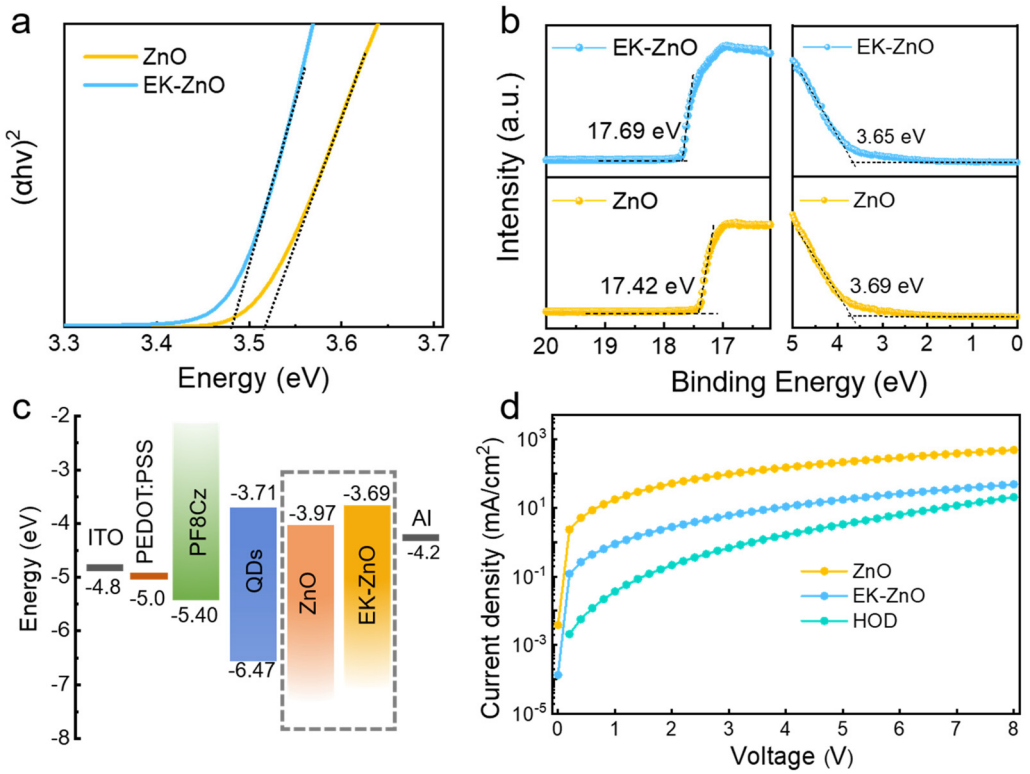

Fig. 3 (a) Tauc plots and (b) UPS spectra of ZnO and EK-ZnO films. (c) Schematic energy level diagram. (d) Current density–voltage characteristics of the electron-only and hole-only devices.

of QDs, which resulted in reduction of space-electron accumulation at the QD/EK-ZnO interface, thereby suppressing the degradation at the QD-ETL junction to enhance the stability.[12] Fig. S6† exhibits the UPS spectra of the QD film on ITO, for which the CBM and valence band maximum were 3.71 and 6.47 eV, respectively. A single-carrier device of electron-only devices (EODs) with a structure of ITO/ETL/QDs/ETL/Al and hole-only devices (HODs) with a structure of ITO/PEDOT:PSS/PF8Cz/QDs/MoO_3/Al were prepared to verify this hybrid configuration (Fig. 3d). The electron current decreased by a unit order of magnitude in EK-ZnO-based QLEDs, much closer to the hole current compared with ZnO-based devices. These results indicate that the upshift CBM of ZnO by additive treatment promotes the balance of charge injection in the QDs.

For further assessment of the effect of EDTAK-modified ZnO NPs on the device performance, blue QLEDs with the structure of ITO/PEDOT:PSS/PF8Cz/QDs/ETL/Al were also fabricated as demonstrated in Fig. 4a. CdSe/ZnSe/ZnS core/shell QDs with a central emission wavelength of 459 nm with full width at half maximum (FWHM) of 25 nm was used as an EML (Fig. S7a†). The photoluminescence quantum yield (PLQY) was about 65%. Fig. S7b† shows the TEM image of CdSe/ZnSe/ZnS QDs with an average size of 10 nm. Normalized EL spectra of QLEDs driven under 3.2 V exhibited pure blue emission at 468 nm without any parasitic contribution from the other neighboring layers (Fig. 4b). The inset of Fig. 4b displays photos of QLEDs operating at 3.2 V, corresponding to the Commission Internationale de l'Eclairage color coordinates of (0.129, 0.068). This illustrates that the charge transport layers have no effect on exciton radiative recombination. Notably, Fig. S8 and S9† exhibit the EL spectra and CIE coordinates of our QLEDs with no obvious change from 2.6 to 5.0 V, indicating substantial stability.

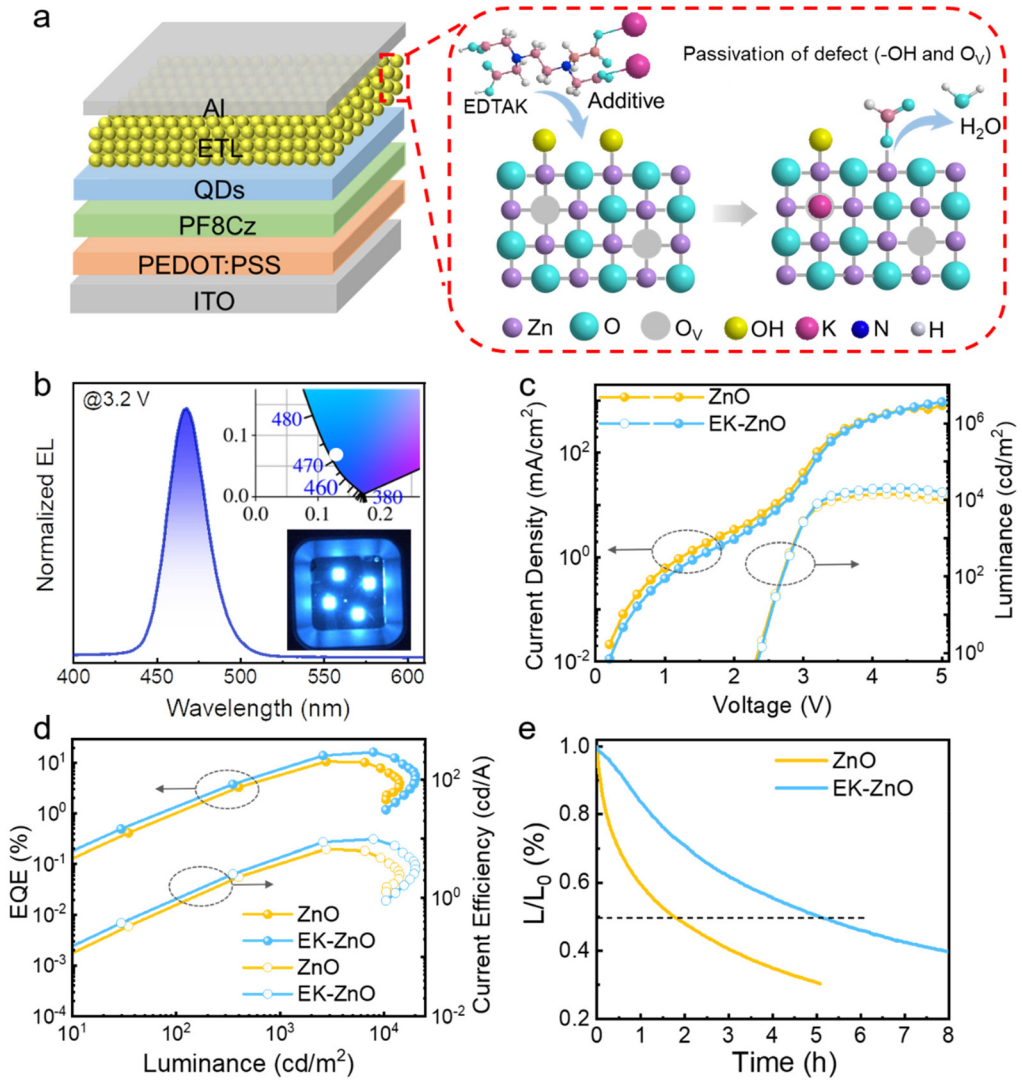

Fig. 4 Device performance. (a) Device structure and schematic illustration of EDTAK-modified ZnO. (b) EL spectrum under 3.2 V bias. Inset: images of the operating devices and the corresponding CIE coordinates. (c) Current density–luminance–voltage characteristics. (d) External quantum efficiency and current efficiency as a function of luminance for the devices based on ZnO and EK-ZnO ETLs. (e) Operational stability data for the two devices.

The current–voltage–luminance (*J*–*V*–*L*), EQE–luminance (EQE–*L*) and current efficiency–luminance (CE–*L*) characteristics of QLEDs based on ZnO and EK-ZnO ETL exhibit lower current density compared with the ZnO-based devices (Fig. 4c and d). The results validated that the electrons injection in EK-ZnO-based devices were less efficient compared with that of the ZnO-based devices, which was ascribed to the increased barrier for electron injection. A considerable increase in luminance was due to restraining Auger recombination by excess electrons.[44] As a result, devices based on EK-ZnO ETL achieved a maximum luminance and peak EQE of 20060 cd m^{-2} and 16.31%, respectively, which were remarkably higher than those (14140 cd m^{-2} and 10.67%) of the ZnO ETL devices (Fig. 1d). The relevant device parameters are summarized in Table 1. Furthermore, a histogram of the maximum EQE of the optimized devices showed that an average EQE of the 18 devices was 15.68% with a low standard deviation of 0.64, suggesting high device reproducibility (Fig. S10†). The operational T_{50} lifetime (when the luminance drops to 50% of its initial value) of EK-ZnO-based QLEDs was found to be 5.05 h at an initial luminance of 3457 cd m^{-2}, equivalent to 1686 h at 100 cd m^{-2} by applying an acceleration factor of 1.64 (Fig. 4d).[5,45] The enhanced T_{50} lifetime for the optimized devices is attributed to reduced Auger recombination and the improved stability of ZnO NPs by EDTAK chelation.[46] Additionally, the excellent stability of EK-ZnO was revealed by keeping ZnO and EK-ZnO solution in an ambient atmosphere with a relative humidity of 35–40% for 3 days, it was clear for EK-ZnO solution, while the ZnO solution became turbid (Fig. S11†).

These systematic analyses and results concluded the improved efficiency of the QLEDs based on the EK-ZnO ETLs, which was attributed to the bifunctional engineering strategy implemented on ZnO using EDTAK. Fig. S12† illustrates the schematic of performance enhancement for devices with primordial ZnO and additive-treatment ZnO films. In the ZnO-based device, the electron transfer barrier was smooth, where excess electrons accumulated at the PF8Cz/QD interface, inducing non-radiative Auger recombination. In addition, the abundant defects (–OH and O_V) on the ZnO surface acted as trap states, inducing exciton quenching, which synergistically reduced the radiation recombination ratio for degrading device performance. Similarly, for the QLED devices based on the EK-ZnO ETL, the carboxyl in EDTAK significantly passivated –OH defects, meanwhile doping K^+ ions passivated O_V in ZnO and the interfacial QDs/ETL, thus suppressing exciton quenching. The chemical interaction contributed to an elevated conduction band energy level of ZnO, increased the electron injection barrier at the ETL/Al cathode and alleviated the electron over-injection, facilitating charge balance. Therefore, the bifunctional surface engineering strategy synergistically enhanced the proportion of radiative recombination, resulting in improved device performance.

Table 1 Summary of the EL performance of QLEDs with ZnO and EK-ZnO ETLs

Device	EL (nm)	V_{on} (V)	L_{MAX} (cd m^{-2})	CE (cd A^{-1})	PE (lm W^{-1})	EQE (%)
ZnO	468	2.4	14 140	6.76	7.08	10.67
EK-ZnO	468	2.4	20 060	9.89	9.71	16.31

3. Conclusions

We report the fabrication of blue QLEDs with high efficiency, high luminance, and extended lifetime using ZnO NPs modified with EDTAK additives as ETLs. Surface engineering passivated the surface defects in ZnO NPs and increased the electron injection barrier energy level. These effects were well reflected in the device performance, which exhibited enhanced charge balance and inhibited exciton quenching, thus increasing effective radiation recombination of QDs. The QLEDs fabricated with EK-ZnO achieved an EQE of 16.31% with outstanding long-operational-lifetime. The remarkable lifetime achieved by suppressing the Auger recombination and the increased stability of ZnO. It is anticipated that this work identifies a new strategy for developing efficient and stable QLEDs for next-generation displays.

4. Experimental section

4.1. Materials and synthesis

4.1.1. Materials. All reagents and materials were used as received without any purification: zinc acetate dihydrate ($Zn(OAc)_2{\cdot}2H_2O$, 99.99%), ethylenediaminetetraacetic acid dipotassium salt (EDTAK, 98%), *n*-octane (98%), dimethyl sulfoxide (DMSO, 99.7%) and tetramethylammonium hydroxide pentahydrate (TMAH, 97%) were purchased from Sigma-Aldrich. The light emission layer (EML) of CdSe/ZnSe/ZnS core–shell QDs was purchased from Suzhou Xingshuo Nanotech Co., Ltd. The PL is of 459 nm with a FWHM of 25 nm, and the PLQY is about 65%. The particle size is about 10 nm. Poly((9,9-dioctylfluorenyl-2,7-diyl)-*alt*-(9-(2-ethylhexyl)-carbazole-3,6-diyl)) (PF8Cz) was purchased from Dongguan Fuan Optoelectronics Technology Co., Ltd.

4.1.2. Synthesis of ZnO and EK-ZnO nanoparticles. $Zn(OAc)_2{\cdot}2H_2O$ was dissolved in 30.0 mL of DMSO with a concentration of 0.1 M as solution A. Tetramethylammonium hydroxide (TMAH) was dissolved in ethanol with a concentration of 0.55 M as solution B. 10 mL of solution B was added dropwise to solution A with a peristaltic pump; the flow rate was 0.47 mL min^{-1}. Then the solution was stirred for 1 h at 20–25 °C with a humidity of 30% to obtain ZnO NPs. Finally, ZnO NPs were centrifuged by using a mixed solvent (1: 1.5) of ethanol and *n*-hexane with a speed of 3000 rpm for 4 min, and re-dispersed in absolute ethyl alcohol with a concentration of 20.0 mg mL^{-1}.

4.1.3. EK-ZnO nanoparticles. $Zn(OAc)_2{\cdot}2H_2O$ was dissolved in 30.0 mL of DMSO with a concentration of 0.1 M as solution A. TMAH was dissolved in ethanol with a concentration of 0.55

M as solution B. 10 mL of solution B was added dropwise to solution A with the same speed of ZnO NPs. 0.8 mL of EDTAK in methyl alcohol with a concentration of 1 mM was added in the mixed solution of A and B with a flow rate of 0.47 mL min^{-1}. It was stirred for 1 h at 20–25 °C with a humidity of 30% to obtain EK-ZnO NPs. EK-ZnO NPs were centrifuged and re-dispersed using the same methods of ZnO NPs, and the concentration was maintained at 20.0 mg mL^{-1}.

4.2. Fabrication of QLEDs

The device structure was glass/ITO/PEDOT:PSS/PF8Cz/QDs/ETLs/Al. The patterned ITO coated glass substrates with a sheet resistance of 23 Ω sq^{-1} were thoroughly cleaned ultrasonically in detergent, deionized water, acetone, and isopropanol for 30 min and then dried, respectively. After cleaning, the ITO glass substrates were treated with UV-ozone for 15 min. After UV-ozone treatment, poly(3,4-ethylenedioxythiophene)/poly(styrene sulfonate) (PEDOT:PSS, AI 4083) solution with a solid content of 1.4% in water was spin-coated on the ITO substrates at 5000 rpm for 45 s and annealed at 140 °C for 15 min. Then, the substrates were transferred into a N_2-filled glovebox. Subsequently, the PF8Cz (8.0 mg mL^{-1} in chlorobenzene) hole transport layer was spin-coated onto the PEDOT:PSS layer at 3000 rpm for 30 s and thermally annealed at 150 °C for 30 min. The CdSe/ZnSe/ZnS core–shell QDs dispersed in *n*-octane (18.0 mg mL^{-1}) and ETLs (ZnO or EK-ZnO NPs 20.0 mg mL^{-1}) were spin-coated at 3000 rpm for 30 s and baked at 60 °C for 30 min. Finally, the device was transferred to a vacuum chamber having a pressure of 5×10^{-6} Torr for Al cathode (100 nm) evaporation. After fabrication, the devices were encapsulated with UV-resin (NOA61 from Norland) inside the N_2-filled glovebox. The cover glass was mounted on top of the QLEDs with UV-resin and then they were cured under intense UV radiation for 1 min. The active area of each device was 0.04 cm^2.

4.3. Characterization methods

Current density–voltage–luminance and the EQE characteristics of the blue QLEDs were analyzed using a characterization system comprising a Keithley 2400 voltmeter together with a Photo Research 735 (PR-735) spectroradiometer under ambient conditions. The XPS measurements were performed using an AXIS SUPRA + System (Shimadzu Inc.) equipped with a monochromatic Al Ka X-ray photon (1486.6 eV) radiation source. The absorption was measured using a Lambda 950 PerkinElmer spectrometer. The PL and TRPL spectra were recorded using a HORIBA FluoroLog-3 spectrofluorometer, respectively. AFM morphology and KPFM analyses were carried out using a SPA400 atomic force microscope. The UPS spectra were recorded using a Thermo Scientific ESCALAB 250 Xi surface-analysis system with a He I discharge lamp (21.22 eV). The operational lifetime T_{50} of the devices was measured using a QLED life test system of Newport Keithley N6705B.

Author contributions

Zuliang Du, Meng Li, and Shujie Wang conceived the idea and proposed the experimental setup. Fensha Cai carried out the initial experimental work and characterization, analyzed the data, and wrote the original draft of the manuscript. Yan Fang, Meng Li, and Xiaohong Jiang provided instructions for the experiments. Yufei Tu and Dadi Tian contributed to optimization of the various experimental steps. Bo Hou and Muhammad Ishaq revised the manuscript. Zuliang Du and Yufei Tu provided financial support and other necessary research resources. All authors reviewed the manuscript and discussed the results.

Conflicts of interest

There are no conflicts to declare.

Acknowledgements

The authors would like to acknowledge the financial support from the National Natural Science Foundation of China (Grant No. U1604261), the Key Scientific Research Project in Colleges and Universities of Henan Province of China (Grant No. 21A416001), and the Key Technologies R&D Program of Henan (Grant No. 232102231038).

References

1 D. Tian, H. Ma, G. Huang, M. Gao, F. Cai, Y. Fang, C. Li, X. Jiang, A. Wang, S. Wang and Z. Du, *Adv. Opt. Mater.*, 2022, **11**, 2201965–2201982.
2 B. Li, M. Lu, J. Feng, J. Zhang, P. M. Smowton, J. I. Sohn, I.-K. Park, H. Zhong and B. Hou, *J. Mater. Chem. C*, 2020, **8**, 10676–10695.
3 A. R. C. Osypiw, S. Lee, S.-M. Jung, S. Leoni, P. M. Smowton, B. Hou, J. M. Kim and G. A. J. Amaratunga, *Mater. Adv.*, 2022, **3**, 6773–6790.
4 M. Liu, N. Yazdani, M. Yarema, M. Jansen, V. Wood and E. H. Sargent, *Nat. Electron.*, 2021, **4**, 548–558.
5 H. Shen, Q. Gao, Y. Zhang, Y. Lin, Q. Lin, Z. Li, L. Chen, Z. Zeng, X. Li, Y. Jia, S. Wang, Z. Du, L. S. Li and Z. Zhang, *Nat. Photonics*, 2019, **13**, 192–197.
6 J. Song, O. Wang, H. Shen, Q. Lin, Z. Li, L. Wang, X. Zhang and L. S. Li, *Adv. Funct. Mater.*, 2019, **29**, 1808377–1808385.
7 Y. Deng, F. Peng, Y. Lu, X. Zhu, W. Jin, J. Qiu, J. Dong, Y. Hao, D. Di, Y. Gao, T. Sun, M. Zhang, F. Liu, L. Wang, L. Ying, F. Huang and Y. Jin, *Nat. Photonics*, 2022, **16**, 505–511.
8 D. Liu, S. Cao, S. Wang, H. Wang, W. Dai, B. Zou, J. Zhao and Y. Wang, *J. Phys. Chem. Lett.*, 2020, **11**, 3111–3115.
9 B.-Y. Lin, W.-C. Ding, C.-H. Chen, Y.-P. Kuo, P.-Y. Chen, H.-H. Lu, N. Tierce, C. J. Bardeen, J.-H. Lee, T.-L. Chiu and C.-Y. Lee, *Chem. Eng. J.*, 2021, **417**, 127983–127990.

10 P. Yu, Q. Yuan, J. Zhao, H. Zhang and W. Ji, *J. Phys. Chem. Lett.*, 2022, **13**, 2878–2884.
11 L. Qian, Y. Zheng, J. Xue and P. H. Holloway, *Nat. Photonics*, 2011, **5**, 543–548.
12 S. Chen, W. Cao, T. Liu, S. W. Tsang, Y. Yang, X. Yan and L. Qian, *Nat. Commun.*, 2019, **10**, 765–773.
13 M. A. Mahmud, N. K. Elumalai, M. B. Upama, D. Wang, A. M. Soufiani, M. Wright, C. Xu, F. Haque and A. Uddin, *ACS Appl. Mater. Interfaces*, 2017, **9**, 33841–33854.
14 L. S. Mende and J. L. MacManus-Driscoll, *Mater. Today*, 2007, **10**, 40–48.
15 E.-H. Jung, B. Chen, K. Bertens, M. Vafaie, S. Teale, A. Proppe, Y. Hou, T. Zhu, C. Zheng and E. H. Sargent, *ACS Energy Lett.*, 2020, **5**, 2796–2801.
16 Q. Su, Y. Sun, H. Zhang and S. Chen, *Adv. Sci.*, 2018, **5**, 1800549–1800555.
17 W. Zhang, X. Chen, Y. Ma, Z. Xu, L. Wu, Y. Yang, S. W. Tsang and S. Chen, *J. Phys. Chem. Lett.*, 2020, **11**, 5863–5870.
18 X. Dai, Z. Zhang, Y. Jin, Y. Niu, H. Cao, X. Liang, L. Chen, J. Wang and X. Peng, *Nature*, 2014, **515**, 96–99.
19 J. Lim, W. K. Bae, D. Lee, S. Lee, C. Lee and K. Char, *ACS Nano*, 2013, **7**, 9019–9026.
20 H. Zhang, N. Sui, X. Chi, Y. Wang, Q. Liu, H. Zhang and W. Ji, *ACS Appl. Mater. Interfaces*, 2016, **8**, 31385–31391.
21 K. Ding, H. Chen, L. Fan, B. Wang, Z. Huang, S. Zhuang, B. Hu and L. Wang, *ACS Appl. Mater. Interfaces*, 2017, **9**, 20231–20238.
22 S. Wang, Y. Guo, D. Feng, L. Chen, Y. Fang, H. Shen and Z. Du, *J. Mater. Chem. C*, 2017, **5**, 4724–4730.
23 H. M. Kim, J. Kim, S. Y. Cho and J. Jang, *ACS Appl. Mater. Interfaces*, 2017, **9**, 38678–38686.
24 Y. Sun, W. Wang, H. Zhang, Q. Su, J. Wei, P. Liu, S. Chen and S. Zhang, *ACS Appl. Mater. Interfaces*, 2018, **10**, 18902–18909.
25 V. Postica, J. Gröttrup, R. Adelung, O. Lupan, A. K. Mishra, N. H. de Leeuw, N. Ababii, J. F. C. Carreira, J. Rodrigues, N. B. Sedrine, M. R. Correia, T. Monteiro, V. Sontea and Y. K. Mishra, *Adv. Funct. Mater.*, 2017, **27**, 1604676–1604690.
26 A. Chen, H. Zhu, Y. Wu, M. Chen, Y. Zhu, X. Gui and Z. Tang, *Adv. Funct. Mater.*, 2016, **26**, 3696–3702.
27 S. Cao, J. Zheng, J. Zhao, Z. Yang, C. Li, X. Guan, W. Yang, M. Shang and T. Wu, *ACS Appl. Mater. Interfaces*, 2017, **9**, 15605–15614.
28 Y. Han, H. Dong, W. Pan, B. Liu, X. Chen, R. Huang, Z. Li, F. Li, Q. Luo, J. Zhang, Z. Wei and C. Q. Ma, *ACS Appl. Mater. Interfaces*, 2021, **13**, 17869–17881.
29 J. Wei, G. Ji, C. Zhang, L. Yan, Q. Luo, C. Wang, Q. Chen, J. Yang, L. Chen and C. Q. Ma, *ACS Nano*, 2018, **12**, 5518–5529.
30 S. Bai, Y. Jin, X. Liang, Z. Ye, Z. Wu, B. Sun, Z. Ma, Z. Tang, J. Wang, U. Würfel, F. Gao and F. Zhang, *Adv. Energy Mater.*, 2015, **5**, 1401606–1401615.
31 Z. Wang, X. Zhu, J. Feng, C. Wang, C. Zhang, X. Ren, S. Priya, S. F. Liu and D. Yang, *Adv. Sci.*, 2021, **8**, 2002860–2002866.
32 X. Liang, S. Bai, X. Wang, X. Dai, F. Gao, B. Sun, Z. Ning, Z. Ye and Y. Jin, *Chem. Soc. Rev.*, 2017, **46**, 1730–1759.
33 Z. Liu, L. Qiu, L. K. Ono, S. He, Z. Hu, M. Jiang, G. Tong, Z. Wu, Y. Jiang, D.-Y. Son, Y. Dang, S. Kazaoui and Y. Qi, *Nat. Energy*, 2020, **5**, 596–604.
34 D. Zhang, T. Guo, J. Zou, Y. Zhou, J. Jin, Z. Zhu, Q. Cao, J. Zhang and Q. Tai, *Small*, 2022, **19**, 2205604–2205614.
35 D. Yang, R. Yang, K. Wang, C. Wu, X. Zhu, J. Feng, X. Ren, G. Fang, S. Priya and S. F. Liu, *Nat. Commun.*, 2018, **9**, 3239–3349.
36 M. Gao, Y. Tu, D. Tian, H. Yang, X. Fang, F. Zhang, H. Shen and Z. Du, *ACS Photonics*, 2022, **9**, 1400–1408.
37 Ü. Özgür, Y. I. Alivov, C. Liu, A. Teke, M. A. Reshchikov, S. Doğan, V. Avrutin, S. J. Cho and H. Morkoç, *J. Appl. Phys.*, 2005, **98**, 041301–041413.
38 J. H. Lin, R. A. Patil, R. S. Devan, Z.-A. Liu, Y.-P. Wang, C.-H. Ho, Y. Liou and Y.-R. Ma, *Sci. Rep.*, 2014, **4**, 6967–6974.
39 M. Chrzanowski, G. Zatryb, P. Sitarek and A. Podhorodecki, *ACS Appl. Mater. Interfaces*, 2021, **13**, 20305–20312.
40 J. Wu, L. Chen, Y. Zhao, Z. Xiong, W. Ji and Y. Lei, *Appl. Phys. Lett.*, 2021, **119**, 073303–073308.
41 R. Azmi, S. Hwang, W. Yin, T.-W. Kim, T. K. Ahn and S.-Y. Jang, *ACS Energy Lett.*, 2018, **3**, 1241–1246.
42 K. Karmakar, A. Sarkar, K. Mandal and G. G. Khan, *ChemElectroChem*, 2018, **5**, 1147–1152.
43 J. Zhang and H. Yu, *J. Mater. Chem. A*, 2021, **9**, 4138–4149.
44 Q. Lin, L. Wang, Z. Li, H. Shen, L. Guo, Y. Kuang, H. Wang and L. S. Li, *ACS Photonics*, 2018, **5**, 939–946.
45 T. Lee, B. J. Kim, H. Lee, D. Hahm, W. K. Bae, J. Lim and J. Kwak, *Adv. Mater.*, 2022, **34**, 2106276–2106284.
46 T. Fang, T. Wang, X. Li, Y. Dong, S. Bai and J. Song, *Sci. Bull.*, 2021, **66**, 36–43.